Stable shapes of three-dimensional vesicles in unconfined and confined Poiseuille flow

Dhwanit Agarwal* and George Biros†
Oden Institute of Computational Engineering and Sciences, University of Texas at Austin, Texas 78712, USA

(Received 1 October 2019; published 28 January 2020)

We use numerical simulations to study the dynamics of three-dimensional (3D) vesicles in unconfined and confined Poiseuille flow. Previous numerical studies have shown that when the fluid viscosity inside and outside the vesicle is the same (no viscosity contrast), a transition from asymmetric slippers to symmetric parachutes takes place as viscous forcing or capillary number is increased. At higher viscosity contrast, an outward migration tendency has also been observed in unconfined flow simulations. In this paper, we study how the presence of viscosity contrast and confining walls affect the dynamics of vesicles and present phase diagrams for confined Poiseuille flow with and without viscosity contrast. To our knowledge, this is the first study that provides a phase diagram for 3D vesicles with viscosity contrast in confined Poiseuille flow. The confining walls push the vesicle towards the center while the viscosity contrast has the opposite effect. This interplay leads to important differences in the dynamics, such as bistability, at high capillary numbers.

DOI: 10.1103/PhysRevFluids.5.013603

I. INTRODUCTION

Vesicles are closed membranes made of a phospholipid bilayer and serve as a model of nucleus free cells such as red blood cells (RBCs). They are filled with fluid and surrounded by fluid. Their high deformability leads to rich shape dynamics in the presence of viscous forcing. Accurate prediction of these shape dynamics when the viscous forcing is generated by a Poiseuille bulk flow is a fundamental problem since this type of background velocity is predominant in biological flows and microfluidics. For example, Poiseuille flow is used for measuring geometric properties of cells [1], for understanding the properties of cell suspensions [2], or for helping in the design of microfluidic devices for sorting cells based on mechanical properties, as in lateral displacement devices [3].

The key parameters that control the shape dynamics are the elastic properties of the membrane, the viscosity contrast (denoted by λ) between the fluid inside and outside the vesicle (both fluids are typically considered to be Newtonian), the confinement (free vs confined flow, and the confinement ratio defined as the ratio of vesicle diameter to the width of confining channel), and the imposed flow parameters, for example, the velocity magnitude. Regarding the elastic properties, vesicles resist bending but have no resistance in shear or shear rate. A dimensionless parameter called capillary number (denoted by C_a) measures the ratio of imposed flow strength over the membrane bending energy and is crucial in the study of the shape dynamics. The vesicle membrane is modeled as locally inextensible so there is a surface tension field that enforces this surface inextensibility. Finally, a key parameter is the reduced volume, ν, of a vesicle, which is the volume of the vesicle over the volume of an equal-area spherical vesicle. If $\nu = 1$ (its maximum value), the vesicle is a sphere that cannot

*dhwanit@oden.utexas.edu
†biros@oden.utexas.edu

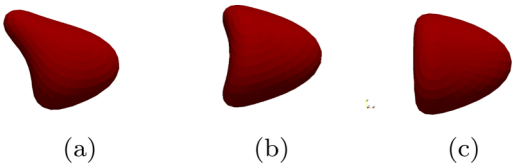

FIG. 1. Different shapes of vesicles. (a) Slipper, (b) Croissant, and (c) Parachute.

deform and behaves as a rigid particle. For $\nu < 1$, the vesicle becomes deformable. Red blood cells (which are not vesicles because they resist shear) in microcirculation have reduced volume of about 0.7 and viscosity contrast of about five.

In Poiseuille flow, a vesicle evolves into some final shape that typically depends on the elastic parameters of the vesicle and the flow parameters. Two well-known shapes are the *parachute* and *slipper* (see Fig. 1). Notice that, depending on the flow conditions, the final state does not need to be stationary. It can be oscillatory: for example *snaking* vesicles observed in confined flows. The Poiseuille flow is symmetric; the parachute shape is also symmetric as the center of mass of the vesicle is at the center line, but, surprisingly, the slipper shape is not symmetric and the center of mass is displaced from the center of the channel. Both shapes were found in one of the earliest experimental studies by Gaehtgens *et al.* [4]. The existence of the slipper shape is mainly attributed to the breakdown of symmetry due to shear gradient in Poiseuille flow. Kaoui *et al.* [5] confirmed the existence of these stable asymmetric slippers using two-dimensional (2D) numerical simulations of a vesicle in unconfined axisymmetric Poiseuille flow and also presented a phase diagram of parachutes and slippers as a function of velocity and reduced volume. The results established that the parachute occurs at higher velocities while slippers dominate at lower velocities. 2D numerical simulations for vesicles of reduced volume 0.6 in confined Poiseuille flow are presented in [6] for viscosity contrast 1. The simulations revealed a much more complex picture as different regimes of confined slipper, unconfined slipper, centered snaking, off-centered snaking, and parachute appeared depending on the confinement and capillary number. The authors in [7] modeled 2D vesicles in confined Poiseuille flow simulations for viscosity contrast 5. The study reveals some important differences in the dynamics when the viscosity contrast is changed from 1 to 5. For example, the authors observed both slipper and parachute shapes at high capillary numbers ($\geqslant$120) depending on initial position of the vesicle.

In three dimensions, a semi-axisymmetric *croissant* shape (as opposed to fully axisymmetric parachute shape; see Fig. 1) has also been observed in recent simulations by Farutin *et al.* [8] in unconfined Poiseuille flow. That study reported a phase diagram similar to [5] for nearly spherical vesicles ($\nu \geqslant 0.9$) with viscosity contrast $\lambda = 1$. The authors observed significant changes in the dynamics at higher viscosity contrast, for example, metastability depending on initial vesicle position and an outward migration tendency.

Coupier *et al.* [9] considered the shapes of 3D vesicles ($\nu \geqslant 0.91$) in confined Poiseuille flow through experiments for viscosity contrast $\lambda = 1$ and high capillary numbers ($\gtrapprox$15). Their study revealed a crossover from a parachute to a bullet shape with increasing reduced volume. This point of crossover (the reduced volume above which bullet shape is observed) was observed to be dependent on capillary number for low confinements (confinement ratio <0.5) while it only depended on confinement ratio at high confinements (confinement ratio $\geqslant$0.5). This indicated that the confinement effects dominate the flow strength above 0.5 confinement ratio. Croissant shapes were also observed for rectangular (as opposed to square) channels.

Contributions. In this paper, we build upon the unconfined flow results in [8] and study, through numerical simulations, the dynamics of 3D vesicle of reduced volume $\nu = 0.90$ with and without viscosity contrast. We reproduce (for validation purposes) the phase diagram for unconfined flow for $\lambda = 1$, present additional slipper shapes for reduced volume $\nu = 0.85$, and study the effects of the

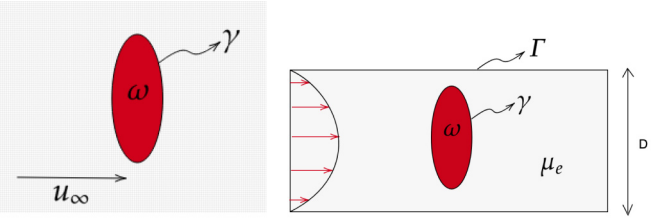

(a) Unconfined flow (b) Confined flow

FIG. 2. (a) Schematic of the domain Ω for unconfined flow. ω denotes the red region enclosed by vesicle membrane γ filled with fluid of viscosity μ_i. The grey region is filled with fluid of viscosity μ_e. u_∞ is the imposed background velocity. (b) Schematic of the domain Ω for confined flow (side view). Γ is the fixed rigid enclosing boundary, which models a channel of circular cross section with axis parallel to the x axis. D is the diameter of the circular cross section. Parabolic flow imposed is shown by red arrows. The grey region is filled with fluid of viscosity μ_e. ω denotes the red region enclosed by vesicle membrane γ filled with fluid of viscosity μ_i.

presence of viscosity contrast on the dynamics. In the unconfined case, we provide a phase diagram in the parameter space of vesicle initial position and capillary number when $\lambda = 5$. For the confined case, we will present phase diagrams in the parameter space of confinement ratio and capillary number for $\lambda \in \{1, 5\}$ and a study of how the confining walls play a pivotal role in determining the dynamics when viscosity contrast is present. We will see how the wall effects and the outward migration due to viscosity contrast lead to coexistence of both slipper and parachute shapes in the confined case. Our results could explain the experiments with RBCs in which slipper shapes are observed at high capillary numbers [10,11]. We will also see that, at high confinement ratio ($\geqslant$0.5), the wall effects dominate causing the vesicle to remain centered with mostly axisymmetric shapes. We also observe two new equilibrium shapes, *bean* and *bell*, in the confined case.

Limitations. It is important to stress here that the vesicles do not have any shear resistance. This makes them different from RBCs which resist shear. Thus, vesicles serve only as a simplistic model of these cells and can have different dynamics compared to the RBCs. We would also like to specify that, for smaller reduced volumes ($\nu \leqslant 0.85$), our numerical scheme is currently unable to resolve the vesicle shapes at high C_a (>10) due to large deformations.

This paper is organized as follows. In Sec. II, we present the problem statement and methodology for both unconfined and confined flows. In Sec. III, we formulate the relevant parameters in both confined and unconfined cases, tabulate the self-convergence results, and verify the correctness of our code by comparing our results and shapes with previous literature. In Sec. IV, we present the results regarding different steady state shapes and behavior of vesicles, including the phase diagram for unconfined flow. In Sec. V, we discuss the results for a vesicle in a confined Poiseuille flow in detail. In Sec. VI, we present the conclusion and further ideas to be explored.

II. PROBLEM FORMULATION AND METHODOLOGY

In this section, we state the flow problem and give its boundary integral formulation. The detailed derivation of this formulation is given in [12]. Table I summarizes the notation used in the paper.

A. Unconfined flow formulation

The formulation for unconfined flow of vesicles is the same as in [13]. In Fig. 2(a), we show the geometric setup for our simulations. In this setup, the fluid flow is governed by the Stokes equation

TABLE I. Index of different symbols.

Symbol	Definition
$\mathbb{S}^2$	Unit sphere
p	Degree of spherical harmonic expansion
γ	Boundary of vesicle
Γ	Fixed rigid boundary
$\mathbf{S}_\gamma$	The single-layer Stokes operator over γ
$\mathbf{D}_\gamma$	The double-layer Stokes operator over γ
$\boldsymbol{u}$	Velocity
$\boldsymbol{u}_\infty$	Background velocity
$\mathbf{f}$	Interfacial force
P	Pressure
t	Time
$\mathbf{n}$	Outward unit normal
μ_i	Viscosity of fluid in vesicle
μ_e	Viscosity of ambient fluid
λ	Viscosity contrast $= \mu_i/\mu_e$
σ	Tension
H	Mean curvature of vesicle
K	Gaussian curvature of vesicle
κ_b	Bending modulus of vesicle membrane
$\boldsymbol{\eta}$	Double layer density on Γ
ω	Volume enclosed by γ
Ω	Volume of interest
R_0	Radius of vesicle
v	Reduced volume of vesicle
C_a	Capillary number
C_n	Confinement ratio

due to negligible effect of inertial forces. The PDE formulation of the flow is as follows:

$$-\mu(\boldsymbol{x})\Delta\boldsymbol{u}(\boldsymbol{x}) + \nabla P(\boldsymbol{x}) = 0 \quad \forall \mathbf{x} \in \mathbb{R}^3\backslash\gamma, \tag{1}$$

$$\mathrm{div}[\boldsymbol{u}(\boldsymbol{x})] = 0 \quad \forall \mathbf{x} \in \mathbb{R}^3\backslash\gamma, \tag{2}$$

$$[[-P\mathbf{n} + (\nabla\boldsymbol{u} + \nabla\boldsymbol{u}^T)\mathbf{n}]] = \mathbf{f} \quad \text{on } \gamma, \tag{3}$$

$$\frac{\partial \mathbf{X}}{\partial t} = \boldsymbol{u}(\mathbf{X}) \quad \forall \mathbf{X} \in \gamma, \tag{4}$$

$$\boldsymbol{u}(\mathbf{x}) \to \boldsymbol{u}_\infty(\mathbf{x}) \quad \text{as } ||\mathbf{x}|| \to \infty, \tag{5}$$

where γ is the vesicle membrane, $\mathbf{u}(\mathbf{x})$ is the velocity of the fluid and $P(\mathbf{x})$ is the pressure. The viscosity μ is given by

$$\mu(\boldsymbol{x}) = \begin{cases} \mu_i & \text{if } \boldsymbol{x} \in \omega, \\ \mu_e & \text{if } \boldsymbol{x} \in \mathbb{R}^3\backslash\omega. \end{cases}$$

$[[l]]$ denotes the jump of quantity l across the vesicle membrane and $\mathbf{n}$ is the outward unit normal to the membrane. Equation (3) is the balance of momentum on the membrane, which requires the surface traction jump to be equal to the total force (denoted by $\mathbf{f}$) exerted by the interface onto the fluid. Equations (4) and (5) enforce a no-slip boundary condition on the vesicle membrane and

set the far field velocity to be the background velocity. We use $\mathbf{X}$ to denote a point on the vesicle membrane γ while $\mathbf{x}$ denotes a point in $\mathbb{R}^3\backslash\gamma$.

The local inextensibility of the vesicle membrane is mathematically equivalent to requiring that the surface divergence of velocity should vanish on the vesicle membrane, i.e.,

$$\mathrm{div}_\gamma[\boldsymbol{u}(\boldsymbol{X})] = 0 \quad \forall \mathbf{X} \in \gamma. \tag{6}$$

Now let us discuss in detail the elastic force $\mathbf{f}$ due to the vesicle membrane elasticity. It comprises a bending and a tension component, the latter being a Lagrange multiplier that enforces the local inextensibility. We denote the bending component by $\mathbf{f}_b$ and the tension component by $\mathbf{f}_\sigma$, so we write

$$\mathbf{f} = \mathbf{f}_b + \mathbf{f}_\sigma. \tag{7}$$

The expressions for these components are (please refer to [14,15] for details)

$$\mathbf{f_b}(\mathbf{X}) = -\kappa_b[\Delta_\gamma H + 2H(H^2 - K))]\mathbf{n}, \tag{8}$$

$$\mathbf{f}_\sigma(\mathbf{X}) = \sigma\,\Delta_\gamma \mathbf{X} + \nabla_\gamma \sigma, \tag{9}$$

where κ_b is the membrane's bending modulus, H and K are the mean and Gaussian curvatures respectively, and σ is the tension at the membrane point $\mathbf{X}$.

Following [12,16], we can rewrite these equations in integral form for $\mathbf{X} \in \gamma$ as follows:

$$\alpha \boldsymbol{u}(\mathbf{X}) = \boldsymbol{u}_\infty(\mathbf{X}) + \mathbf{S}_\gamma[\mathbf{f_b} + \mathbf{f}_\sigma](\mathbf{X}) + \mathbf{D}_\gamma[\boldsymbol{u}](\mathbf{X}), \tag{10}$$

$$\mathrm{div}_\gamma[\boldsymbol{u}(\mathbf{X})] = 0, \tag{11}$$

$$\frac{\partial \mathbf{X}}{\partial t} = \boldsymbol{u}(\mathbf{X}), \tag{12}$$

where $\alpha := (1+\lambda)/2$. The single-layer convolution integral is defined as $\mathbf{S}_\gamma[f](\mathbf{x}) := \int_\gamma S_0(\mathbf{x},\mathbf{y})\mathbf{f}(\mathbf{y})d\gamma$, with

$$S_0(\mathbf{x},\mathbf{y}) = \frac{1}{8\pi\mu}\frac{1}{||\mathbf{r}||}\left(I + \frac{\mathbf{r}\otimes\mathbf{r}}{||\mathbf{r}||^2}\right),$$

where $\mathbf{r} := \mathbf{x} - \mathbf{y}$, I is the identity operator, $\otimes$ is the tensor product, and $||\cdot||$ is the Euclidean norm. The double-layer convolution integral is defined as $\mathbf{D}_\gamma[f](\mathbf{x}) := \int_\gamma D_0(\mathbf{x},\mathbf{y})\mathbf{f}(\mathbf{y})d\gamma$, with

$$D_0(\mathbf{x},\mathbf{y}) = \frac{-3(1-\lambda)}{4\pi}\left((\mathbf{r}\cdot\mathbf{n})\frac{\mathbf{r}\otimes\mathbf{r}}{||\mathbf{r}||^5}\right).$$

Discretization .We use spherical harmonics discretization for $\mathbf{X}$ and functions defined on γ. The singular quadratures described in [13] are used to evaluate the integrals. The system of equations (10)–(12) is then solved using a semi-implicit scheme [13] for the velocity $\mathbf{u}$ and tension σ. Vesicle position, $\mathbf{X}$, is then updated as $\mathbf{X}_{\mathrm{new}} = \mathbf{u}\Delta t + \mathbf{X}_{\mathrm{old}}$, where Δt is the time step.

B. Confined flow formulation

We define vesicle radius, denoted by R_0, to be the radius of a sphere that has the same volume as the vesicle. We set $R_0 = 2$ in our simulations. To model the flow of a vesicle in confined Poiseuille flow, we create a channel with length much larger than the vesicle radius and a circular cross section. In our simulations, we set the length of the channel to be eight times the vesicle radius R_0. The axis of the channel is parallel to the x axis, and vesicle starts slightly displaced in the y direction from the axis of the channel. Refer to Fig. 2(b) for a general representation of the setup. The boundary integral formulation that accounts for confinement is the 3D extension of the formulation discussed in [17]. To account for the confinement, we add the vesicle-wall interaction term to the right-hand

side of Eq. (10) and append one more equation, (15), for the calculation of the unknown double layer density $\boldsymbol{\eta}$ on the fixed rigid boundary Γ. The formulation becomes

$$\alpha \boldsymbol{u}(\mathbf{X}) = \mathbf{S}_\gamma[\mathbf{f_b} + \mathbf{f}_\sigma](\mathbf{X}) + \mathbf{D}_\gamma[\boldsymbol{u}](\mathbf{X}) + \mathbf{D}_\Gamma[\boldsymbol{\eta}](\mathbf{X}), \tag{13}$$

$$\mathrm{div}_\gamma[\boldsymbol{u}(\mathbf{X})] = 0 \quad \forall \mathbf{X} \in \gamma, \tag{14}$$

$$\mathbf{U}(\mathbf{x}) = -\frac{1}{2}\boldsymbol{\eta}(\mathbf{x}) + \mathbf{S}_\gamma[\mathbf{f_b} + \mathbf{f}_\sigma](\mathbf{x}) + \mathbf{D}_\gamma[\boldsymbol{u}](\mathbf{x}) + \mathbf{D}_\Gamma[\boldsymbol{\eta}](\mathbf{x}) + \mathbf{N}_0[\boldsymbol{\eta}](\mathbf{x}) \quad \forall \mathbf{x} \in \Gamma, \tag{15}$$

$$\frac{\partial \mathbf{X}}{\partial t} = \boldsymbol{u}(\mathbf{X}) \quad \forall \mathbf{X} \in \gamma, \tag{16}$$

where $\mathbf{N}_0[\boldsymbol{\eta}](\mathbf{x}) = \mathbf{n}(\mathbf{x}) \int_\Gamma [\mathbf{n}(\mathbf{y}) \cdot \boldsymbol{\eta}(\mathbf{y})] ds(\mathbf{y})$ and $\mathbf{U}(\mathbf{x})$ is the given velocity of rigid enclosing boundary at $\mathbf{x} \in \Gamma$. We solve the system of equations (13) and (14) for $\mathbf{u}$ and σ as in the unconfined case. We then use the obtained $\mathbf{u}$ and σ in (15) to solve for double-layer density $\boldsymbol{\eta}$ on Γ. Finally, Eq. (16) is discretized as $\mathbf{X}_{\text{new}} = \mathbf{u}\Delta t + \mathbf{X}_{\text{old}}$ to solve for new vesicle position $\mathbf{X}_{\text{new}}$. To avoid the effect of finite length of the channel, after each time step we translate the vesicle so that the x coordinate of the center of the vesicle coincides with the x coordinate of the center of the channel. Each simulation typically takes about 10 000 time steps and 15 hours of wall clock time.

III. SIMULATION SETUP AND PARAMETERS

In this section, we describe the simulation setup and list the relevant input and output parameters, which we monitor to study the dynamics of vesicles in both unconfined and confined cases.

A. Unconfined flow parameters

A vesicle is characterized by its reduced volume v, which is defined as the ratio of the volume of the vesicle to a sphere with the same area as the vesicle. It is given by

$$v := 6\pi^{1/2} V A^{-3/2},$$

where V and A are the volume and surface area of the vesicle respectively. The imposed background fluid flow $\boldsymbol{u}_\infty = (v_x, 0, 0)$ is an axisymmetric Poiseuille profile given by

$$v_x = \alpha(D^2/4 - y^2 - z^2) \tag{17}$$

in Cartesian coordinates, where D is the diameter of the Poiseuille flow and α is the curvature of the flow. The vesicle starts slightly displaced in the y direction from the centerline of Poiseuille flow. We use the dimensionless capillary number for Poiseuille flow given by

$$C_a := \frac{\alpha R_0^4 \mu_e}{\kappa_b}, \tag{18}$$

where κ_b is the bending modulus of the vesicle as specified in the Sec. II A. C_a measures the flow strength over the bending energy of the membrane. We take $R_0 = 2$, $D = 20R_0$, $\mu_e = 1$, and $\kappa_b = 1$ in our simulations[1] and vary the flow curvature α to vary the capillary number C_a. Although the flow is unconfined, we can measure the degree of confinement using the dimensionless confinement ratio (C_n), defined as $C_n := \frac{2R_0}{D}$. Since D and R_0 are fixed, $C_n = 0.1$ in our unconfined flow simulations. The viscosity contrast $\lambda := \mu_i/\mu_e$ is the ratio of the viscosity of the fluid inside the vesicle to the viscosity of the outside fluid and is crucial in determining vesicle dynamics. We study the vesicle dynamics for a range of capillary numbers and reduced volumes with $\lambda = 1$ and $\lambda = 5$.

[1]If the unit of length is micrometers (μm), the unit of mass is micrograms (μg), and the time is in seconds (s), then $R_0 = 2$ μm, $\kappa_b = 10^{-21}$ J, $\mu_e = 10^{-3}$ Pa s. Then if the flow curvature is $\alpha = 1$ in our simulation, it corresponds to a Poiseuille flow with a maximum velocity of 400 μm/s.

TABLE II. Self-convergence results for unconfined and confined flow. p is the order of spherical harmonics discretization. We regard $p = 48$ as the ground truth and calculate error relative to it.

p	Rel. error (unconfined flow)	Rel. error (confined flow)
6	4.1×10^{-3}	6×10^{-2}
12	6×10^{-5}	4×10^{-3}
24	1.2×10^{-5}	1.5×10^{-4}

B. Confined flow parameters

In our simulations of confined flow, the diameter of the channel is denoted by D. The velocity of the rigid boundary Γ is denoted by $\mathbf{U}(\mathbf{x})$ [refer to Fig. 2(b)]. We impose the Poiseuille velocity profile with diameter of the flow equal to D. To do this, we set the velocity of the rigid boundary,

$$\mathbf{U}(\mathbf{x}) = (v_x, 0, 0), \qquad \text{where } \mathbf{x} = (x, y, z) \text{ and } v_x = \alpha(D^2/4 - y^2 - z^2),$$

in Eq. (15). We use capillary number C_a, reduced volume v, and viscosity contrast λ as defined earlier. We also use a dimensionless parameter called confinement ratio (C_n), given by

$$C_n = \frac{2R_0}{D},$$

to characterize the extent of confinement. The higher the C_n is, the closer the bounding walls are to the vesicle. We study the vesicle dynamics for a range of capillary numbers and confinement ratios.

C. Steady state and convergence results

To determine if a steady state is reached, we monitor the lateral displacement of the vesicle center (Y_g), bending energy of the vesicle ($E_b := \int_\gamma \frac{1}{2}\kappa_b H^2 d\gamma$), and its volume moments tensor [$\mathbf{I} := \int_\omega (||\hat{\mathbf{r}}||^2 I - \hat{\mathbf{r}} \otimes \hat{\mathbf{r}}) dV$, where $\hat{\mathbf{r}} = \mathbf{r} - \mathbf{r_0}$, $\mathbf{r_0}$ is the center of the vesicle and I is the identity tensor]. We say that the vesicle has reached a steady state when these observables reach a steady state or their dynamics become nearly periodic. Such oscillatory behavior is actually the typical scenario in our simulations.

To verify the correctness of our code, we report the self-convergence results in a variety of different settings. First, we consider the unconfined setting for fixed physical parameter values of $v = 0.90$, $C_a = 5$, and $\lambda = 1$. In this scenario, we compare the position of the vesicle center for spherical harmonics discretization of order $p = 6$, 12, 24, and 48 after several thousand time steps. We regard the simulation with $p = 48$ as the baseline and compute the relative error in the position of vesicle's center as a function of spherical harmonics order p. We repeat this for confined flow with $v = 0.90$, $C_n = 0.5$, $C_a = 5$, and $\lambda = 1$. The results are summarized in Table II.

To further verify the correctness, we present the steady state shapes of our simulations of unconfined flow for $v = 0.9$, $\lambda = 1$ with $C_a = 4$, 14, and 28 in Figs. 3, 4, and 5 respectively. In

(a) (b)

FIG. 3. Unconfined flow with $v = 0.90$, $C_a = 4$, $\lambda = 1$. Tank treading slipper. (a) Side view of slipper and (b) Rear view of slipper.

(a) (b)

FIG. 4. Unconfined flow with $\nu = 0.90$, $C_a = 14$, $\lambda = 1$. Semiaxisymmetric croissant shape. No tank treading. (a) Side view of croissant and (b) Rear view of croissant.

these simulations, we obtained three shapes, namely (1) tank-treading off-centered slipper (called TT slipper), (2) non-tank-treading slightly off-centered croissant, and (3) non-tank-treading centered parachute. These shapes and results are consistent with the numerical and experimental results presented in [8,9] and we view them as an additional validation of our code [see Fig. 9(a)]. In the case when we obtain a slipper shape, i.e., when $C_a = 4$, we obtain periodic oscillations of vesicle position while bending energy remains constant (see Fig. 8). An axisymmetric bullet shape with a flat rear (as opposed to the concave rear in the parachute shape) is obtained for $\nu = 0.96$, $C_a = 500$, $\lambda = 1$ shown in Fig. 6. We also present the steady state shape obtained for unconfined flow simulation with a vesicle of reduced volume $\nu = 0.65$ for $\lambda = 1$ and $C_a = 1.8$ in Fig. 7. The shape obtained is similar to the one presented in [18]. We observe periodic oscillations of slipper shape about a mean position in this case as well.

IV. RESULTS FOR UNCONFINED FLOW

A. Viscosity contrast $\lambda = 1$

We use this study of unconfined flow with no viscosity contrast (i.e., $\lambda = 1$) as a validation of our code, as these results have been reported in [8]. In the unconfined Poiseuille flow simulations for reduced volumes $\nu = 0.90$ and 0.95, *slipper*, *croissant* and *parachute* shapes are observed as C_a is increased. Slippers (Fig. 3) are asymmetric, off-centered, and exhibit tank-treading motion. Croissants (Fig. 4) are slightly off-centered and semi-axisymmetric while parachutes (Fig. 5) are centered and fully axisymmetric. In particular, for $\nu = 0.95$, slippers are observed in the range $0.46 \leqslant C_a \leqslant 1.4$, croissants are observed in the range $1.4 < C_a \leqslant 4$, and parachutes are observed in the range $C_a > 4$. For $\nu = 0.90$, slippers are observed in the range $0.46 \leqslant C_a \leqslant 4$, croissants are observed in the range $4 < C_a \leqslant 15$, and parachutes are observed in the range $C_a > 15$. We observe that decreasing the reduced volume causes the transitions from slipper to croissant and croissant to parachute to occur at higher C_a. For $\nu = 0.85$, our code was able to resolve shapes for $C_a \leqslant 10$ and we observed only slipper shapes. Simulating a 3D vesicle of reduced volume $\nu < 0.90$ in Poiseuille flow is a hard problem and we are not aware of any study that provides its full dynamics as a function of C_a. We combine all these results to plot a phase diagram for unconfined flow in parameter space of reduced volume (ν) and capillary number (C_a), shown in Fig. 9(a). The scaled equilibrium lateral

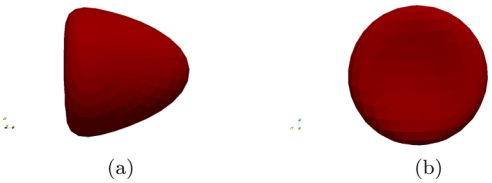

(a) (b)

FIG. 5. Unconfined flow with $\nu = 0.90$, $C_a = 28$, $\lambda = 1$. Centered axisymmetric parachute shape. No tank treading. (a) Side view of parachute and (b) Rear view of parachute.

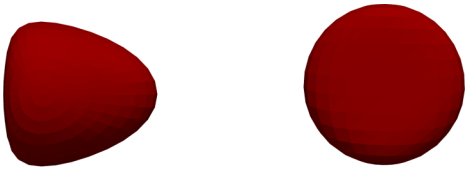

(a) (b)

FIG. 6. Unconfined flow with $\nu = 0.96$, $C_a = 500$, $\lambda = 1$. Centered axisymmetric bullet shape. No tank treading. (a) Side view of bullet and (b) Rear view of bullet.

positions of the vesicle center (Y_g/R_0) for different reduced volumes plotted against C_a, are presented in Fig. 9(b). We note that Y_g is reduced with increasing C_a till it becomes zero and stays there afterwards for $\nu \geqslant 0.90$. For $\nu = 0.85$, the same behavior is observed for Y_g. Our results are in line with the analytical studies [19,20], numerical studies [8,21], and the available experiments [9,22]. In particular, the simulation results in [8] and the experimental results in [9] are also plotted for comparison in Fig. 9(a) after proper scaling of capillary numbers. The slight quantitative difference in the our results compared to the simulations in [8] could be due to the difference in the radius of the Poiseuille flow, which is not mentioned in [8].

B. Viscosity contrast $\lambda = 5$

When we set the viscosity contrast to $\lambda = 5$, some important differences in dynamics are observed depending on the vesicle initial position. We denote the vesicle center's initial distance from the centerline of the flow by Y_{g_0}. When the vesicle starts close to the center (i.e., $Y_{g_0} = 0.025R_0$) for $\nu = 0.90$ and $\lambda = 5$, slippers, croissants, and parachutes are observed as C_a is increased but with different ranges compared to $\lambda = 1$ case. We observe slippers for $0.46 \leqslant C_a \leqslant 5$, croissants for $7 \leqslant C_a < 18$, and parachutes for $C_a \geqslant 18$. These observations suggest that increasing the viscosity contrast causes the shape transitions to occur at higher C_a. A similar observation was made in [7] using 2D vesicle simulations. In the transition phase from slipper to croissant, for example at $C_a = 6$, we found a special regime in which the vesicle oscillates between the slipper and croissant shapes, something that does not happen in flows without viscosity contrast ($\lambda = 1$).

When the initial position of the vesicle is chosen far from the centerline (say, $Y_{g_0} = 1.5R_0$), an outward migration is observed for $0.46 \leqslant C_a \leqslant 1350$. The observations agree with the results in [8], which reported this outward migration tendency due to the viscosity contrast. At fixed viscosity contrast, the critical value of Y_{g_0}, above which outward migration is observed, depends on both capillary number and reduced volume. The higher the capillary number is, the lower is the critical initial position above which outward migration occurs. For example, for $\nu = 0.90$ and $C_a = 0.46$, this critical value is observed to be $1.08R_0$ while for $\nu = 0.90$ and $C_a = 1350$ outward migration occurs for $Y_{g_0} > 0.05R_0$ (see Fig. 11 for a complete picture of $\nu = 0.90$ with $\lambda = 5$). Also, the higher the reduced volume is, the higher is the critical initial position for outward migration. For example, when $\nu = 0.95$ and $C_a = 1350$, this critical initial vesicle position is observed to be $0.5R_0$. For $\nu = 0.85$, we expected a lower value of critical initial position but, surprisingly, we observe

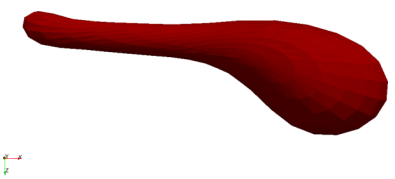

FIG. 7. Unconfined flow simulation $\nu = 0.65$, $C_a = 1.8$, $\lambda = 1$. Tank treading slipper shape.

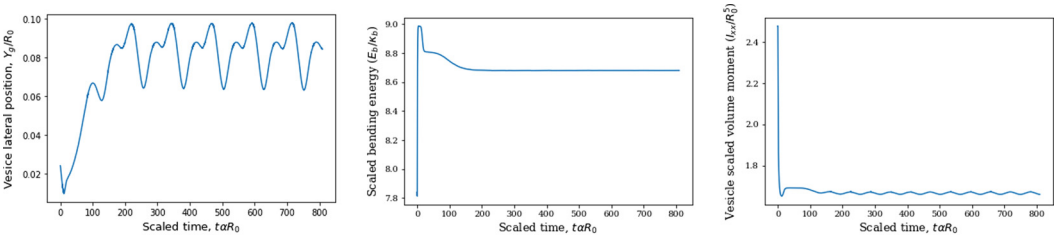

FIG. 8. Periodic oscillations in vesicle position and moment in unconfined flow simulation with $\nu = 0.90$, $\lambda = 1$, $C_a = 4$. (a) Vesicle center (Y_g) scaled with R_0. (b) Bending energy of vesicle with time. (c) Vesicle moment about flow axis with time. Bending energy remains constant after some time. Equilibrium shape is a slipper.

outward migration even for the very low value of $Y_{g_0} = 0.025R_0$ at all $C_a \geqslant 0.46$. We speculate that this happens because the equilibrium slipper positions of vesicles of reduced volume $\nu = 0.85$ are so high that they exceed the critical initial position for outward migration even at low C_a [see the equilibrium positions in the $\lambda = 1$ case shown in Fig. 9(b)]. Thus, causing an outward migration even at very low capillary numbers.

Although the exact reason for outward migration tendency remains unclear, our simulations reveal that the transient inclination angles (with respect to flow direction) of a migrating vesicle can differentiate outward vs inward migration. The dependence of lift on the orientation of the vesicle with respect to flow has also been discussed before in [23]. In our simulations, outward migration is associated with lower values of inclination angles while inward migration is associated with higher values of inclination angles. Higher viscosity contrast leads to lower inclination angles and, thus, a strong outward migration tendency (see Fig. 10). The figure also indicates that starting far away from the center leads to lower inclination angles, thus to an increased outwards migration tendency. A further study in the direction of calculating normal stress difference as in [24] could shed further light on this phenomenon.

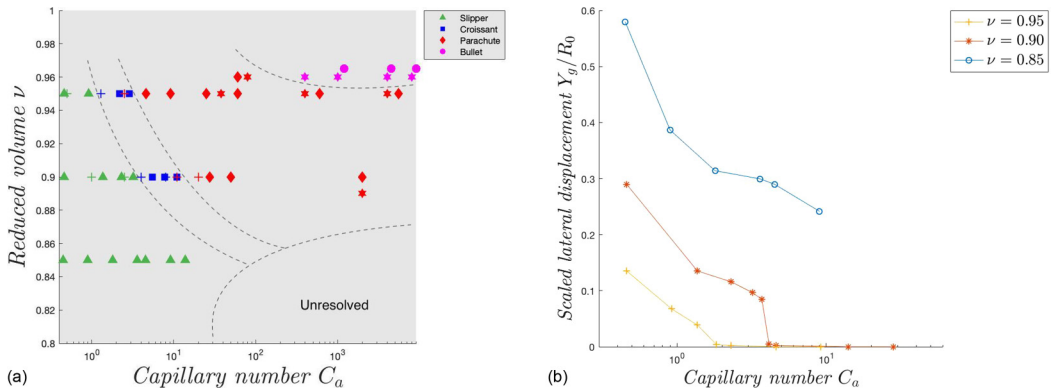

FIG. 9. Phase diagram and equilibrium lateral positions for unconfined flow with $\lambda = 1$. (a) A phase diagram for unconfined flow with $\lambda = 1$, showing equilibrium shapes in different regions of vesicle reduced volume ν and capillary number C_a. Green denotes slipper, blue denotes croissant, red denotes parachute, and magenta denotes bullet. Triangles, squares, diamonds, and circles denote our simulations. Hexagrams denote experimental low confinement results in [9] and + denote simulation results in [8]. The unresolved regime is the range of parameter values for which our code was unable to resolve the shapes. Dashed black curves are guides for the eye. (b) Scaled equilibrium lateral positions vs capillary number for unconfined flow.

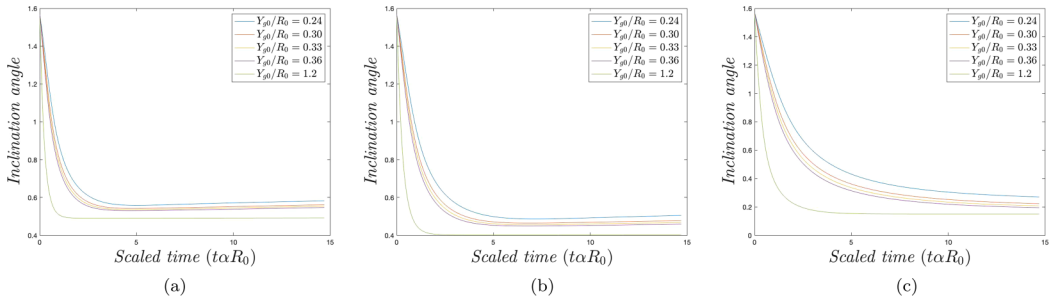

FIG. 10. Plot of vesicle transient inclination angle (in radians; with respect to flow direction) vs migration for different initial positions in unconfined flow at $C_a = 3.2$. Higher viscosity contrast and higher initial lateral positions lead to lower inclination angles. Outward migration is correlated to lower inclination angles. (a) $\lambda = 1$, (b) $\lambda = 2$, and (c) $\lambda = 5$.

C. Discussion of results for unconfined flow

The results for $\lambda = 1$ are fairly straightforward. The equilibrium lateral position keeps on decreasing with increasing C_a and finally becomes zero. For $\lambda = 5$, the initial position changes the dynamics and it is evident that there is an outward migration tendency, which opposes the inward migration due to the quadratic component of the Poiseuille flow. When the vesicle initial position is far enough from the centerline, this outward migration tendency dominates and causes an overall outward migration velocity. Also, the lower the reduced volume is, the more dominant this outward migration seems to be. The question is, do these observations apply to the confined flow case? This is what we try to answer in the next section.

V. RESULTS FOR CONFINED FLOW

In this section, we study the effect of wall confinement (see Fig. 12) on vesicle dynamics. We first study the case with no viscosity contrast for different confinement ratios. Then we proceed onto the case with viscosity contrast. We use a vesicle of reduced volume $\nu = 0.90$ for this study and compare it with unconfined flow dynamics.

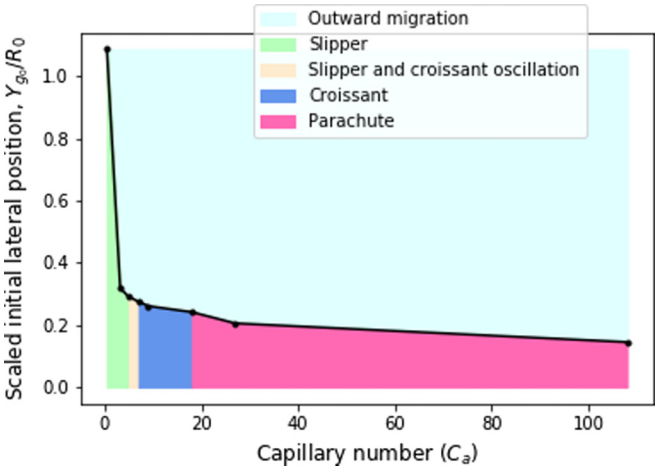

FIG. 11. Unconfined flow phase diagram for vesicles of reduced volume $\nu = 0.90$ with $\lambda = 5$ in the parameter space of initial vesicle position (Y_{g_0}) and capillary number (C_a). For viscosity contrast $\lambda = 5$, the vesicle dynamics also depend on the initial position of the vesicle.

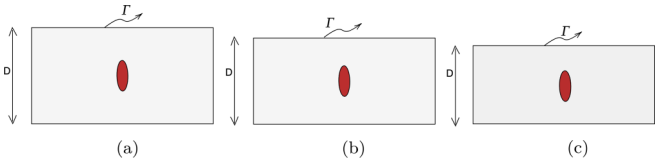

FIG. 12. Different confinement ratios (C_n). Γ is the channel with diameter D. The vesicle is denoted in red. High confinement ratio means the bounding walls are closer to the vesicle. (a) $C_n = 0.3$, (b) $C_n = 0.5$, (c) $C_n = 0.7$.

A. Viscosity contrast $\lambda = 1$

First, we consider the case of low confinement ratio, i.e., $C_n = 0.3$. In this case, it is natural to expect that the difference between the confined and the unconfined Poiseuille flows would be negligible due to the weak hydrodynamic effect of the walls. Hence, we should expect the same qualitative behavior as in the unconfined case. The simulations indeed confirm our expectation. We observe slippers (Fig. 13) in the range $1 \leqslant C_a \leqslant 4.5$ with equilibrium lateral position decreasing as C_a increases. In the range $4.5 \leqslant C_a \leqslant 13$ croissants are observed, and parachutes are observed for $C_a > 13$.

But, increasing the confinement ratio to 0.5 paints a different picture. A centered bell shape (see Fig. 14) is observed for $0.134 \leqslant C_a \leqslant 3$. The bell shape is axisymmetric like the parachute shape but the rear is convex, i.e., it bulges outwards in contrast to the concave rear in the parachute shape. Note that initially the bell seems to exhibit *snaking* motion, but after some time the motion dies and a centered stationary bell is observed (see Fig. 15). For $C_a > 3$, the rear of the shape becomes concave and we get a parachute. On further increasing the confinement ratio to $C_n = 0.7$, a centered bell shape is observed in the range $0.5 \leqslant C_a \leqslant 2.5$ and a parachute shape is observed for $C_a > 2.5$. The occurrence of axisymmetric centered shapes at low C_a suggests a dominance of the effects of confining walls which push the vesicle towards the centerline.

B. Viscosity contrast $\lambda = 5$

Based on our earlier results, we expected this to be the most interesting case since the inward push from the confining walls (for details on wall push, refer to [22,23,25]) and the outward migration tendency (due to the viscosity contrast) oppose each other and can result in interesting dynamics. And indeed that is the case. For low confinement ratio $C_n = 0.3$, if the vesicle initial position is close to centerline ($Y_{g_0} \leqslant 0.04R_0$), we observe a slipper shape for $0.05 \leqslant C_a \leqslant 5$, a croissant for $5 \leqslant C_a \leqslant 10$, and a parachute for $10 \leqslant C_a \leqslant 680$ similar to the no-contrast case. But, interestingly, for $C_a \geqslant 100$, a bistability is observed, i.e., slipper and parachute equilibrium shapes coexist depending on initial position of the vesicle. For example, for $C_a = 682$, if a vesicle starts far away from the centerline ($Y_{g_0} > 0.30R_0$), the equilibrium shape is a tank-treading slipper at mean position $Y_g = 0.38R_0$, while if it starts close to center the equilibrium shape is a centered parachute (see Fig. 16). To ascertain if this coexistence occurs because of the cancellation of outward migration

FIG. 13. Confined flow: slipper shape with $\nu = 0.90$, $\lambda = 1$, $C_n = 0.3$, $C_a = 1.5$. (a) Side view and (b) Rear view.

(a) (b)

FIG. 14. Confined flow: bell shape with $\nu = 0.90$, $\lambda = 1$, $C_n = 0.5$, $C_a = 0.5$. (a) Side view and (b) Rear view.

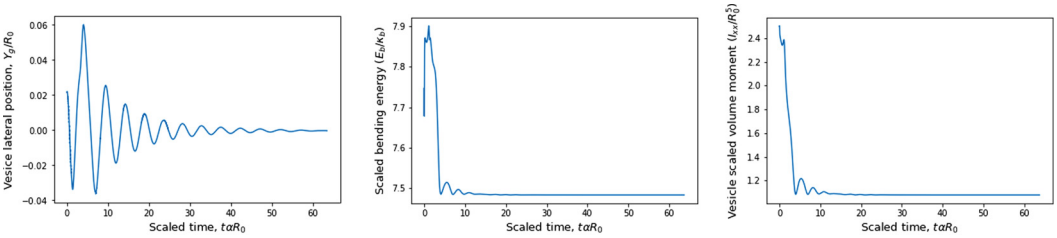

(a) (b) (c)

FIG. 15. Vesicle dynamics for confined flow simulation with $\nu = 0.90$, $\lambda = 1$, $C_a = 0.5$, $C_n = 0.5$. (a) Vesicle center (Y_g) scaled with R_0. (b) Bending energy of vesicle vs time. (c) Vesicle moment about flow axis vs time. The equilibrium shape is a bell. Snaking oscillations die down eventually.

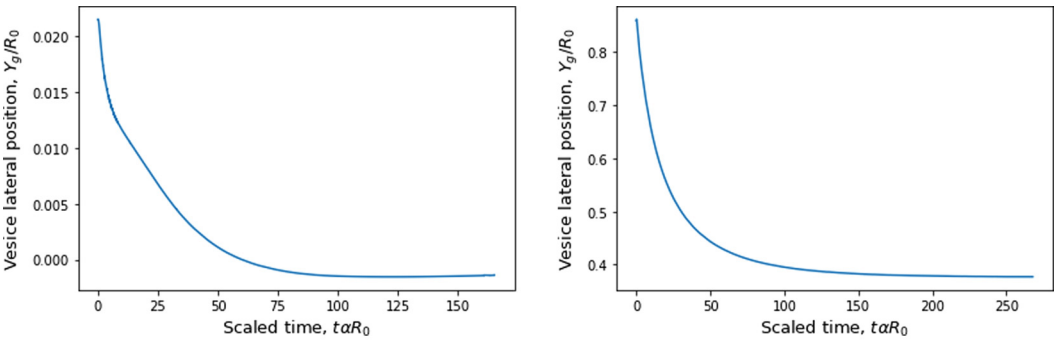

(a) (b)

FIG. 16. Vesicle lateral position [vesicle center (Y_g) scaled with R_0] for confined flow simulation with $\nu = 0.90$, $\lambda = 5$, $C_a = 682$, $C_n = 0.3$. Coexistence of slipper and parachute. (a) Vesicle starts close to center: initial position $Y_{g_0} = 0.022R_0$. Equilibrium shape is a centered parachute. (b) Vesicle starts far from center: initial position $Y_{g_0} = 0.85R_0$. Equilibrium lateral distance is nonzero and equilibrium shape is a slipper.

(a) (b)

FIG. 17. Confined flow: bean shape with $\nu = 0.90$, $\lambda = 5$, $C_n = 0.5$, $C_a = 0.27$. (a) Side view and (b) Rear view.

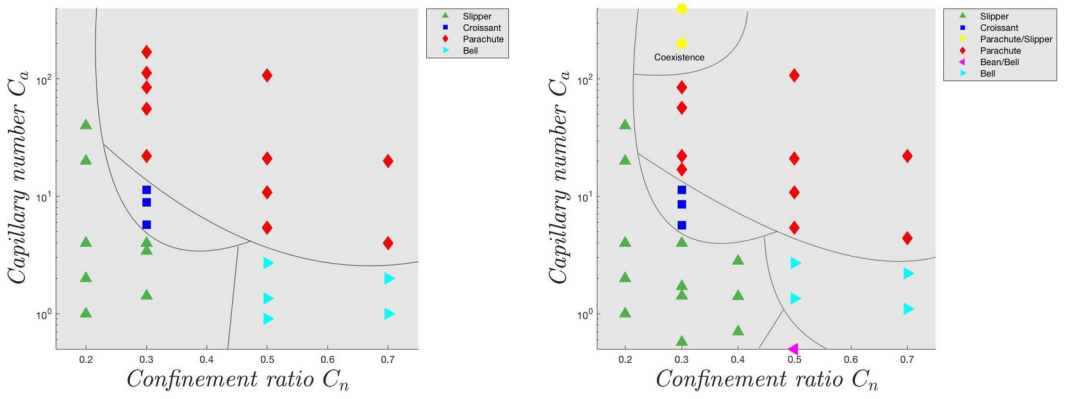

FIG. 18. Phase diagrams for confined flow in the parameter space of confinement ratio C_n and capillary number C_a. (a) Confined flow with $\lambda = 1$. (b) Confined flow with $\lambda = 5$. Black curves are guides for the eye.

tendency by the confinement effects, we repeat the simulation with initial position slightly less than the equilibrium slipper position but without confining walls. We observe that, for the same parameters without confining walls, the vesicle continues to migrate outwards perpetually, while it stops at an equilibrium position when confining walls are present. This confirms that this bistability is a result of the cancellation of outward migration tendency by the confinement effects. We have seen that outward migration is strong at high C_a in unconfined flow simulations, which could explain why no such bistability is observed for $C_a < 100$.

For $C_n = 0.5$, the confinement effects dominate, as observed in the no-viscosity-contrast case. Although we do not observe coexistence of slipper and parachute in this case, we do observe a coexistence of bean (see Fig. 17) and bell shapes for $0.1 \leqslant C_a \leqslant 0.4$ depending on the initial position. The reason for this bistability remains unclear. For $0.4 < C_a < 4$, only the bell shape is observed, while parachute is observed for $C_a \geqslant 4$. For $C_n = 0.7$, bell and parachute shapes are observed as before when C_a is increased.

C. Discussion of results for confined flow

We combine the above results for confined flow without and with viscosity contrast in the parameter space of capillary number and confinement ratio to plot the phase diagrams in Fig. 18. We conclude that, for low confinement ratio, the dynamics is largely similar to that in the unconfined flow. Slipper shapes are common in low confinements, although parachutes are also observed at high flow strength. Interestingly, the presence of viscosity contrast induces a bistability at high flow strength, i.e., both slippers and parachutes are observed. At higher confinement ratios ($C_n \geqslant 0.5$), confinement effects dominate the dynamics and axisymmetric shapes (bell and parachute) are observed. While with $\nu = 0.90$ we do not observe coexistence of slipper and parachute in higher confinements, we should keep in mind that lower reduced volume vesicles might exhibit this coexistence, since the outward migration tendency seems to become stronger as reduced volume is decreased. This could be a possible explanation for the experimental observation of slipper shapes of RBCs in microcapillaries at high velocities which have reduced volume of about 0.7 and viscosity contrast of about 5 [10,11].

VI. CONCLUSION AND FUTURE WORK

In this paper, we have used vesicles as a model of RBCs to provide a picture of their dynamics and equilibrium shapes in confined Poiseuille flow with and without viscosity contrast. The phase

diagrams for both the cases have been provided. To our knowledge, this is the first study that provides a phase diagram for 3D vesicles with viscosity contrast in confined Poiseuille flow. We have seen how the parabolic velocity profile of Poiseuille flow, viscosity contrast, and the confining walls affect the dynamics and shapes of vesicles for a range of relevant parameters. Although in the case with no viscosity contrast we have seen that the slipper shape occurs on decreasing the flow strength, the experiments with RBCs point to the opposite effect. Our results on the bistability created due to the presence of viscosity contrast and the confining walls could explain this anomaly. But, unlike RBCs, vesicles have no shear resistance, which leads to large deformations. It should be interesting to study how the dynamics of capsules (which have shear resistance) compares between vesicles in unconfined and confined Poiseuille flows. This is a future direction that we aim to explore in our future work.

[1] F. Merola, P. Memmolo, L. Miccio, R. Savoia, M. Mugnano, A. Fontana, G. D'Ippolito, A. Sardo, A. Iolascon, A. Gambale, and P. Ferraro, Tomographic flow cytometry by digital holography, Light Sci. Appl. **6**, e16241 (2017).

[2] V. Vitkova, M.-A. Mader, B. Polack, C. Misbah, and T. Podgorski, Micro-macro link in rheology of erythrocyte and vesicle suspensions, Biophys. J. **95**, L33 (2008).

[3] E. Henry, S. H. Holm, Z. Zhang, J. P. Beech, J. O. Tegenfeldt, D. A. Fedosov, and G. Gompper, Sorting cells by their dynamical properties, Sci. Rep. **6**, 34375 (2016).

[4] P. Gaehtgens, C. Dührssen, and K. H. Albrecht, Motion, deformation, and interaction of blood cells and plasma during flow through narrow capillary tubes, Blood Cells **6**, 799 (1980).

[5] B. Kaoui, G. Biros, and C. Misbah, Why Do Red Blood Cells Have Asymmetric Shapes Even in a Symmetric Flow? Phys. Rev. Lett. **103**, 188101 (2009).

[6] B. Kaoui, N. Tahiri, T. Biben, H. Ez-Zahraouy, A. Benyoussef, G. Biros, and C. Misbah, Complexity of vesicle microcirculation, Phys. Rev. E **84**, 041906 (2011).

[7] N. Tahiri, T. Biben, H. Ez-Zahraouy, A. Benyoussef, and C. Misbah On the problem of slipper shapes of red blood cells in the microvasculature, Microvasc. Res. **85**, 40 (2013).

[8] A. Farutin and C. Misbah, Symmetry breaking and cross-streamline migration of three-dimensional vesicles in an axial Poiseuille flow, Phys. Rev. E **89**, 042709 (2014).

[9] G. Coupier, A. Farutin, C. Minetti, T. Podgorski, and C. Misbah, Shape Diagram of Vesicles in Poiseuille Flow, Phys. Rev. Lett. **108**, 178106 (2012).

[10] G. Tomaiuolo, M. Simeone, V. Martinelli, B. Rotoli, and S. Guido, Red blood cell deformation in microconfined flow, Soft Matter **5**, 3736 (2009).

[11] S. Guido and G. Tomaiuolo, Microconfined flow behavior of red blood cells in vitro, C. R. Phys. **10**, 752 (2009).

[12] C. Pozrikidis, *Boundary Integral and Singularity Methods for Linearized Viscous Flow* (Cambridge University Press, Cambridge, 1992).

[13] D. Malhotra, A. Rahimian, D. Zorin, and G. Biros, A parallel algorithm for long-timescale simulation of concentrated vesicle suspensions in three dimensions (preprint available at https://pdfs.semanticscholar.org/da58/d664941a3b0a563c598a2256c4ea3454fc4e.pdf) (unpublished).

[14] C. Pozrikidis, Effect of membrane bending stiffness on the deformation of capsules in simple shear flow, J. Fluid Mech. **440**, 269 (2001).

[15] J. L. Weiner *et al.*, On a problem of Chen, Willmore, Indiana Univ. Math. J. **27**, 19 (1978).

[16] C. Pozrikidis, Interfacial dynamics for Stokes flow, J. Comput. Phys. **169**, 250 (2001).

[17] A. Rahimian, S. Veerapaneni, and G. Biros, Dynamic simulation of locally inextensible vesicles suspended in an arbitrary two-dimensional domain, a boundary integral method, J. Comput. Phys. **229**, 6466 (2010).

[18] A. Farutin, T. Biben, and C. Misbah, 3D numerical simulations of vesicle and inextensible capsule dynamics, J. Comput. Phys. **275**, 539 (2014).

[19] G. Danker, P. M. Vlahovska, and C. Misbah, Vesicles in Poiseuille Flow, Phys. Rev. Lett. **102**, 148102 (2009).
[20] A. Farutin, T. Biben, and C. Misbah, Analytical progress in the theory of vesicles under linear flow, Phys. Rev. E **81**, 061904 (2010).
[21] B. Kaoui, G. H. Ristow, I. Cantat, C. Misbah, and W. Zimmermann, Lateral migration of a two-dimensional vesicle in unbounded Poiseuille flow, Phys. Rev. E **77**, 021903 (2008).
[22] G. Coupier, B. Kaoui, T. Podgorski, and C. Misbah, Non-inertial lateral migration of vesicles in bounded Poiseuille flow, Phys. Fluids **20**, 111702 (2008).
[23] P. Olla, The lift on a tank-treading ellipsoidal cell in a shear flow, J. Phys. II (France) **7**, 1533 (1997).
[24] G. Ghigliotti, A. Rahimian, G. Biros, and C. Misbah, Vesicle Migration and Spatial Organization Driven by Flow Line Curvature, Phys. Rev. Lett. **106**, 028101 (2011).
[25] I. Cantat and C. Misbah, Lift Force and Dynamical Unbinding of Adhering Vesicles under Shear Flow, Phys. Rev. Lett. **83**, 880 (1999).